Lossless Matching Layer for Silicon Lens Arrays At 500 GHz Using Laser Ablated Structures

Bueno Lopez, Juan ; Bosma, Sjoerd ; Bußkamp-Alda, Tobias ; Alonso Del Pino, Maria; Llombart, Nuria

DOI
10.1109/TTHZ.2022.3202031

Publication date
2022

Document Version
Final published version

Published in
IEEE Transactions on Terahertz Science and Technology

Lossless Matching Layer for Silicon Lens Arrays at 500 GHz Using Laser Ablated Structures

Juan Bueno, Sjoerd Bosma, *Student Member, IEEE*, Tobias Bußkamp-Alda, Maria Alonso-delPino, *Senior Member, IEEE*, and Nuria Llombart, *Fellow, IEEE*

***Abstract*—We present the design, fabrication and characterization of a broadband lossless matching layer for silicon lens arrays. The proposed matching layer is based on silicon frusta (truncated pyramids) on top of the lens array fabricated by means of laser ablation. This matching layer is advantageous over quarter-wavelength dielectric matching layers since it covers more than an octave of bandwidth. We compare the performance of this matching layer with the commonly-used parylene-C matching layer at the center of the targetted band (500 GHz) in a lens-antenna integrated system. We measure a 1.6 dB higher transmission of the proposed silicon frusta matching compared to the parylene-C matching layer.**

***Index Terms*—Anti-reflection coating, dielectric lens antennas, matching layer, submillimeter-wave.**

I. Introduction

SILICON is widely used for submillimeter-wave integrated lens antennas [1], [2], [3]. However, the high permittivity of silicon ($\varepsilon_r^{Si} = 11.9$) results in high reflection at the lens-air interface. These reflections negatively impact the sidelobes [3], [4] decrease the gain [4] and have a strong impact on the input impedance [5].

Numerous antireflection coatings (AR coatings, also known as matching layers) have been developed to limit these reflections [6], [7], [8], [9]. Single-layer thin-films of parylene-C ($\varepsilon_r = 2.62$) [6], SUEX ($\varepsilon_r = 2.86$) [7], Cirlex ($\varepsilon_r = 3.37$) [8] and a mixture of Stycast 1266 ($\varepsilon_r = 2.82$) and Stycast 2850FTJ ($\varepsilon_r = 4.84$) [9] were successfully used at these frequencies as quarter-wavelength impedance transformers, since their relative permittivity is close to that of an ideal quarter-wavelength transformer $\sqrt{\varepsilon_r^{Si}} = 3.45$. Multiple dielectric matching layers were used in [4], [10] to increase the transmission bandwidth.

However, the coating materials themselves may incur additional dielectric losses, which may not be negligible at submillimeter wavelengths, and the deposition of the thin films is costly. Furthermore, the adhesion of the matching layers to the silicon lens can be difficult, especially for cryogenically cooled lenses.

Periodic subwavelength structures imprinted in a dense material (silicon) have been also widely used as matching layers [11], [12], [13], [14], [15], [16], [17], [18], [19], [20]. Several fabrication techniques, such as deep-reactive ion etching (DRIE) [11], [12], [13], dicing technique [14], [15], [16], [17], and laser ablation [18], [19] have been proposed and used at THz frequencies.

DRIE was used in [11], [12], and [13] to create an antireflective coating on flat silicon wafers but has, to our best knowledge, never been demonstrated on a curved surface (i.e., silicon lens), which might not be straightforward.

A dicing saw technique was used in [14], [15], and [16] to create impedance transformers on both flat silicon surfaces and silicon lenses. Reflection and/or transmission measurements were performed at frequencies up to 300 GHz but the authors conclude that this technique is not scalable to higher frequencies.

The laser ablation technique has two main advantages over a dicing saw method: the smallest achievable dimension is set by the laser ($\sim$1–2 μm) whereas the dicing blade width is $\sim$20–100 μm; and the laser spot can be tuned, allowing a smooth taper of the frusta walls in comparison with the fixed width of available dicing saws. The combination of these two advantages allows a broader frequency transmittance coverage reaching frequencies up to a few THz, which is not possible with the dicing saw fabrication.

In fact, laser ablation has been used to create continuous impedance on a flat silicon wafer [18] and on alumina lenses [19]. The authors reported the transmittance and/or reflectance of periodic sub-wavelength structures at frequencies up to 700 GHz. However, a direct comparison between the radiation performance of a quarter-wavelength AR coating and a continuous impedance-transforming matching layer in an integrated silicon lens-antenna architecture has not been presented before at these high frequencies, where the beam pattern, the directivity and the gain are measured.

Another potential advantage of the laser ablation is that, since the lens and the matching layer are made of the same material, the antireflective coating will not suffer from thermal stress when cryogenically cooled. Similar structures made on alumina have been successfully tested cryogenically [19], and there is no reason why the frusta matching layer presented in this article could not be used as a broadband matching layer for cryogenically cooled lens arrays.

Manuscript received 21 April 2022; revised 22 June 2022 and 12 August 2022; accepted 17 August 2022. Date of publication 26 August 2022; date of current version 7 November 2022. This work was supported by the ERC Starting Grant LAA-THz-CC 639749. *(Corresponding author: Juan Bueno.)*

Juan Bueno is with the Electronic Circuits and Architectures group, Delft University of Technology, 2628 CD Delft, The Netherlands (e-mail: j.buenolopez@tudelft.nl).

Sjoerd Bosma, Maria Alonso-delPino, and Nuria Llombart are with the Terahertz Sensing Group, Delft University of Technology, 2628 CD Delft, The Netherlands (e-mail: s.bosma@tudelft.nl; m.alonsodelpino@tudelft.nl; n.llombartjuan@tudelft.nl).

Tobias Bußkamp-Alda is with the Veld Laser Innovations B.V., 7041 GB 'S-Heerenberg, The Netherlands (e-mail: tbusskamp@veldlaser.nl).

Color versions of one or more figures in this article are available at https://doi.org/10.1109/TTHZ.2022.3202031.

Digital Object Identifier 10.1109/TTHZ.2022.3202031

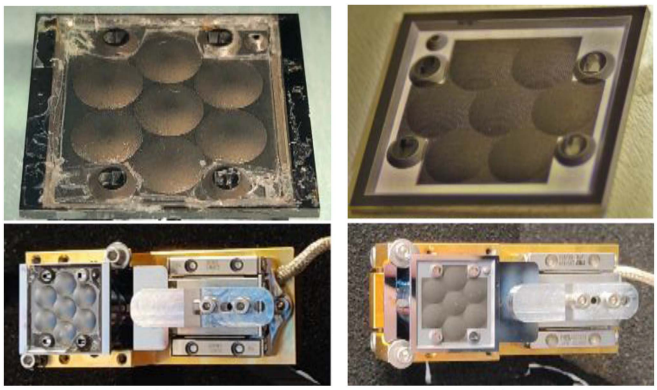

(a) (b)

Fig. 1. Silicon lens arrays. (a) Parylene-C (top) and assembled antenna (bottom). (b) Frusta matching layer (top) and assembled antenna (bottom).

TABLE I
FRUSTA DIMENSIONS AND LASER PARAMETERS

Frusta dimensions		
	Designed	Fabricated
d [μm]	40	32 ± 5
p [μm]	108	109 ± 5
h [μm]	127	149 ± 10
α [deg]	15	14 ± 2
Laser fabrication parameters		
Average power	7 W	
Spot size	25 μm	
Pulse duration	<12 ps	
Repetition rate	200 kHz	

In this article, we compare the performance of the silicon leaky-wave lens antenna that was demonstrated in [20] with a quarter-wavelength AR coating to a continuous impedance-transforming matching layer. We have fabricated and measured two otherwise identical silicon lens antennas (see Fig. 1) with different matching layers: a quarter-wavelength AR coating of parylene-C and a periodic structure consisting of flat-topped square pyramids (frusta) in silicon. We measure an improved gain of 1.4–2.0 dB at 450–500 GHz using the pyramid matching layer compared to the parylene-C AR coating.

II. Lens Matching Layer Design

We compare the simulated performance of two matching layers on the silicon lens antenna described in [20] in the operational bandwidth of this antenna of 450–650 GHz: a quarter-wavelength (94 μm) layer of parylene-C and a periodic arrangement of subwavelength flat-topped square pyramids (frusta) in silicon.

The frusta are fabricated using laser ablation, which is performed by Veld Laser Innovations B.V. (www.veldlaser.nl). Laser ablation is the process in which material from a surface is removed by a pulsed laser beam. The material, in the case of this lens array silicon, is locally heated by the absorbed laser energy and evaporates or sublimates. The laser pulses are very short, of the order of a few tens of picoseconds, causing only minimal material damage during processing due to the ultrashort light-matter interaction making it suitable for microfabrication.

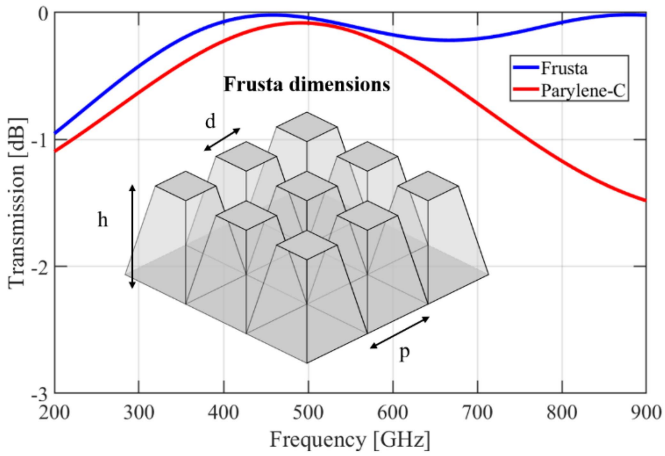

Fig. 2. Simulated transmission of both the parylene-C and the periodic matching layer. The inset inside the figure is a sketch of the simulated periodic frusta used as the matching layer.

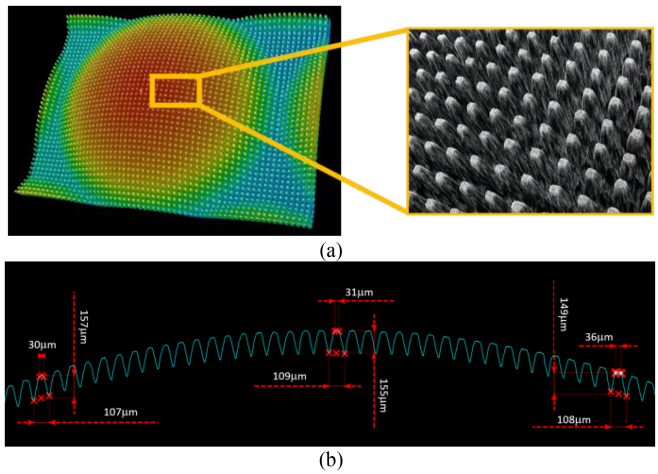

Fig. 3. (a) Scale 2:1. 3-D image of a lens and zoomed view of the frusta taken with a confocal microscope. (b) Scale 1:1. Measurement of the frusta dimensions using the cross section along the center of the lens array.

Due to the small dimensions of the pyramids, this microfabrication technique has two constraints that need to be considered for the design: it is not possible to carve straight walls in the silicon. The minimum angle that can be obtained for these specific pyramid dimensions is 13°. However, this is not a problem since the tapered walls increase the bandwidth; it is very difficult to reliably manufacture the pyramid-ends in a sharp point at the top for the entire lens array. We therefore decided to truncate the top of the pyramids and make frusta instead.

Considering these constraints, we thus design the frusta, as indicated in the inset of Fig. 2. These dimensions are given in [21] for a higher frequency design (2 THz) and have been scaled to 500 GHz to meet our frequency band. The design values can be given in Table I.

The transmission at the interface between the silicon lens and free space is simulated for a frustum unit cell for broadside incidence using CST. The reflection coefficient at broadside is an accurate approximation for such very shallow silicon lens arrays. A full-wave periodic structure simulation is performed to

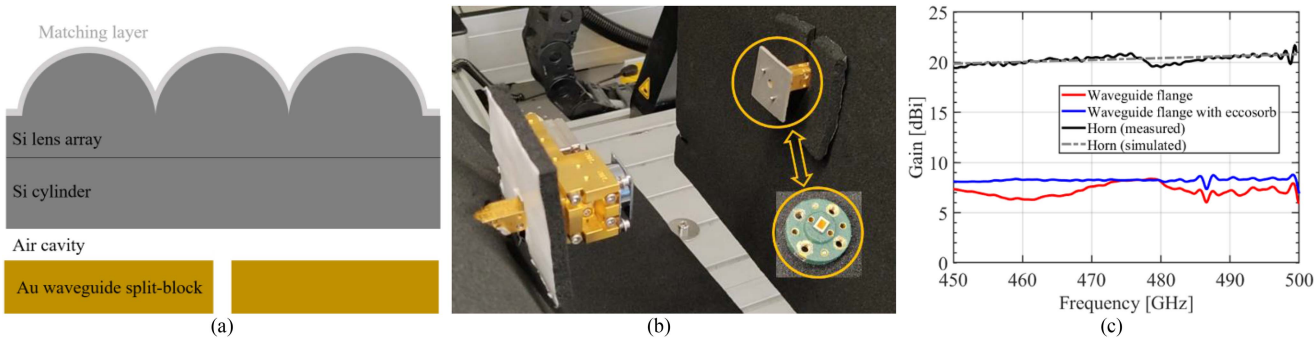

Fig. 4. (a) Schematic of the antenna assembly. (b) Measurement setup. Either an open-ended waveguide flange with eccosorb around it (for pattern measurements) or a horn antenna (for gain measurements) are used on the second extender, as indicated by the arrow. (c) Measured gain of the waveguide flange with and without the eccosorb and the measured and simulated gain of the horn.

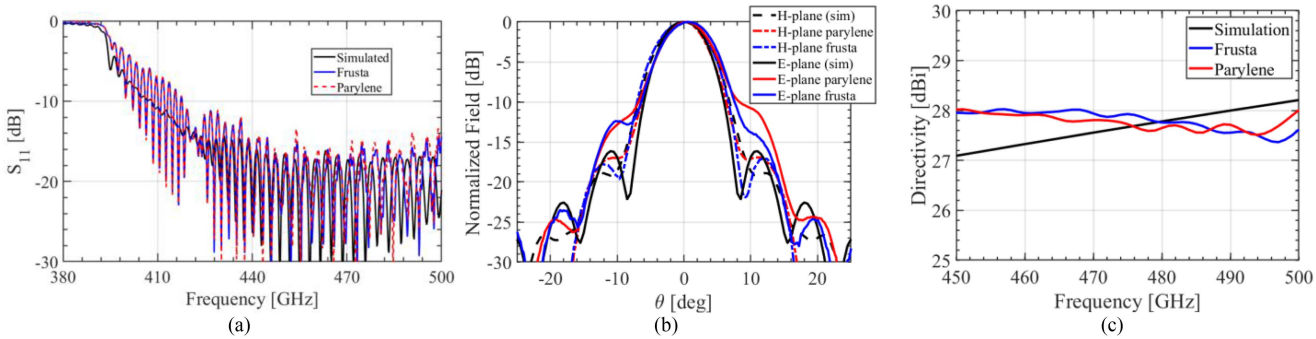

Fig. 5. (a) Simulated and measured S_{11} of both antennas. (b) Simulated and measured beam patterns at a frequency of 480 GHz. (c) Simulated and measured directivity of both antennas.

obtain the transmission for the frusta structure; for the parylene-C matching layer, an equivalent transmission line was used, assuming lossless parylene-C. The simulated transmission is given in Fig. 2 and is better than -0.3 dB for both structures in the center of the band but the parylene-C matching layer transmission decays for lower and higher frequencies whereas the pyramid matching layer stays fairly constant for the full bandwidth. The radiation patterns of the lens antennas are simulated using the Fourier Optics methodology [22], which was also used in [20], assuming a quarter-wavelength matching layer with $\varepsilon_r = 2.62$. The simulated radiation patterns are shown in Fig. 5(b).

III. Fabrication and Characterization of the Periodic Frusta Matching Layer

The lens array with frusta matching layer is fabricated in two steps. These two fabrication steps are performed in the same laser setup, but with two different settings. First, the entire lens array is manufactured thicker than the thickness of the nominal lens. This extra thickness corresponds exactly to the height of the frusta. The lens array geometry is made using an imported 3-D file. Second, this extra thickness is locally removed to form the frusta. For this step, a 2-D file containing the grid from which the excess material will be removed from the lenses is loaded into the laser ablating setup. Dedicated optics move the focus of the laser along the shape of the lens and the frusta are carved by passing the laser several times over the lens surface to obtain the correct depth. The parameters used by the laser for the fabrication of the frusta are given in Table I. Conformal carving is not possible at this point using our current setup since it can only move along three axis (x-, y-, and z-axis) and the laser cannot follow the lens profile. This limits the application of the ablation fabrication technique to shallow lenses (i.e., lenses in which only the top part of the lens is illuminated). To apply this technique to more curved lenses, two routes could be investigated: the current laser setup could be modified and the number of axes could be increased to five (x-, y-, z-, θ-, and ψ-axis) so the laser can follow the lens profile; and a new frusta design that takes the angle of incident along the profile of the lens surface into consideration. This new design would have to adjust vertically the length of the frusta (h) to ensure high transmission for non-broadside angles.

After fabrication, the shape of the frusta is measured in three-dimensional (3-D) using a confocal microscope [see Fig. 3(a)]. The 3-D image can be sliced and used to measure the profile of the frusta, and therefore obtain their period [see Fig. 3(b)], dimension of the top flat part [see Fig. 3(c)] and height [see Fig. 3(d)]. The shape of the frusta is measured at three different locations (left, middle, and right) in the two perpendicular planes. The shape of each frustum along these cuts is measured and its average valued can be given in Table I, together with the fabrication accuracy and designed values. The small difference between the designed and fabricated frusta moves the center of the frequency band slightly (about 10%), but the design is so broadband that this shift does not affect the overall performance of the frusta matching layer. Furthermore, the accuracy in the fabrication process of the frusta matching layer is similar to the accuracy of the parylene-C thickness during its deposition process (5% to 20% thickness variation depending on the location of the lens array in the deposition chamber).

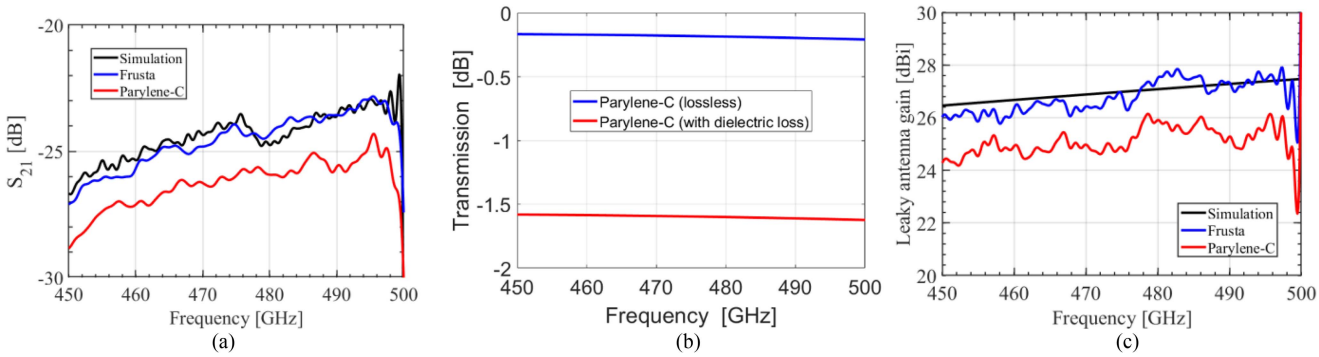

Fig. 6. (a) Simulated and measured S_{21} of the antenna with both matching layers. (b) Simulated loss of the parylene-C matching layer when dielectric loss is added. (c) Simulated and measured gain of the antenna with both matching layers. Note that the gain difference between the pyramids matching layer and the parylene-C matching layer is explained by the 1.6 dB dielectric loss of the parylene-C.

IV. Antenna Assembly and Measurement Setup

The lens arrays with the two different matching layers are integrated and measured one-by-one in a lens antenna fed by a high-efficiency leaky-wave feed described in [20]. Although seven lenses are fabricated in each array, only the central element is excited. The antenna assembly is extensively explained in [20], and consists of a gold-plated waveguide split block with a WR-1.5 waveguide flange on the bottom and a waveguide transition to a square (362 μm) aperture at the top. Next, two silicon wafers are placed on the block containing the leaky-wave cavity and transformer layer. The height of the lens is achieved with a solid cylindrical block of silicon placed on top of the wafers. Finally, either the lens array with the parylene-C or with the pyramid structures is placed on this silicon block. A piezoelectric motor is used to align the lens array with the feed as in [20]. A sketch of the assembled antenna is shown in Fig. 4 and a photograph of the assembled antenna with the two different lens arrays is shown in Fig. 1.

We measure the antenna at 450–500 GHz using a VNA and two WR-2.2 frequency extenders. The antenna under test is in a fixed position and the receiving antenna is placed in a three-axis CNC stage, and they are both facing each other. The 2-D antenna patterns are measured in an angle of 30° around broadside in the far field at a distance of 10 cm distance. The patterns are measured using an open-ended waveguide flange with eccosorb material surrounding the waveguide aperture on the flange, similar to [23]. The absorber on the flange greatly reduces the oscillations that are measured due to the presence of the waveguide flange and can be interchanged with a horn antenna, as shown in Fig. 4(b). The gain of the flange is measured with and without the absorber and is shown in Fig. 4(c). The gain of the waveguide with the absorber is much less oscillatory. We use the horn antenna, with a gain of around 20 dB, to measure the gain of the antennas under test in the far field. The gain of this horn is separately measured to be in good agreement with the specified gain from the manufacturer (Flann Microwave), also shown in Fig. 4(c). We later use this measured gain to characterized the gain of the antennas under test.

V. Measurements and Results

We compare the simulated and measured reflection coefficient ($S11$) of both antennas in Fig. 5(a). The antenna is well-matched above 425 GHz, the agreement with simulations is good, and the reflections in the $S11$ are not noticeably different for the two prototypes. The measured and simulated reflection coefficient do not match below 425 GHz because the leaky lens antenna that we use for the characterization of the frusta matching layer has a bandwidth between 450 and 650 GHz, and the cut-off frequency of the waveguide is around 400 GHz. The measured radiation patterns are compared to the simulated patterns at 480 GHz in Fig. 5(b). The measurements are in reasonable agreement with the simulated patterns. The measured patterns from the parylene-C and frusta matching layer are very similar, indicating similar directivity. Indeed, the measured directivity, which is obtained by integrating the 2-D patterns and shown in Fig. 5(c), is nearly the same for both prototypes and is also in agreement with the simulated directivity. The array coupling and cross-polarization have not been measured but, although it cannot be directly extracted from the directivity measurements [see Fig. 5(c)], the fact that the parylene-C and frusta directivities are nearly identical suggests that both matching layers are performing similarly in terms of array coupling and cross-polarization. Moreover, the fabricated frusta layer is symmetric, having same response for TE/TM polarization. Therefore, we expect not to have any impact on the cross-polarization.

We use Friis' equation to simulate the coupling between the antenna and horn (S_{21}) at broadside at a distance of 10 cm. To remove the effect of multiple reflecting waves in the measurement setup, we apply a time gate to the measured S_{21} that filters out these reflections after the first received time-domain pulse. The simulated S_{21} takes into account the loss in the gold-plated split block ($\sigma = 3.5 \times 10^6$) and the simulated gain. As shown in Fig. 6(a), the simulated coupling is between -27 and -23 dB at 450–500 GHz. The measured coupling is in very good agreement for the frusta matching layer but $\sim$1.6 dB lower for the parylene-C matching layer. This difference can be explained by the dielectric loss present in the parylene-C [see Fig. 6(b)], where we use an absorption coefficient of 35cm^{-1} [24], [25], [26]. The measured gain is evaluated from the measured S_{21} [see Fig. 6(a)] and the measured horn gain [see Fig. 4(c)] removing the loss in the waveguide block. The comparison between the simulated and measured gain is shown in Fig. 6(c), and is above 26 dBi for the frusta matching layer and above 24 dBi for the parylene-C matching layer.

VI. Discussion

The fabricated lens arrays are the same, except for the matching layer on top. The measured results in Fig. 6(c) show that the gain of the periodic frusta matching layer is higher than for the parylene-C matching layer, suggesting a better performance as an AR coating of the periodic frusta structure. This difference in performance is not due to a difference in impedance match or directivity, as demonstrated in Fig. 4(c). Both matching layers perform similarly in term of S_{11}, and we thus associate the gain difference to the dielectric loss in the parylene-C. In fact, an absorption coefficient of 35 cm^{-1} explains the difference in gain, as demonstrated in Fig. 6(b). Although the reported values for absorption coefficient vary largely in the literature, our modeled absorption coefficient is within the reported values. For example, an absorption coefficient of 27 cm^{-1} is reported in [24] at frequencies between 1 and 3 THz for parylene-C whereas and the reported value above 6 THz was 75 cm^{-1} in [25] for parylene-N. These values are in line with the value that we assume in our analysis although lower values have also been found 2 cm^{-1} and 16 cm^{-1} at 450 GHz and 2.8 THz, respectively [26].

VII. Conclusion

We compare the performance at submillimeter wavelengths of two different matching layers on the same silicon leaky-wave lens antenna arrays. The fabricated antennas are the same with the exception for the matching layer. The first is a quarter-wavelength parylene-C antireflecting coating and the second a continuous impedance-transforming matching layer which is realized by periodic subwavelength frusta features laser-ablated directly on the lens surface. We describe the laser machining process to manufacture the frusta suitable for silicon lens arrays. We characterize both antennas in terms of reflection coefficient, radiation patterns (directivity) and gain and compare these results to high-frequency simulations. The measured performance from both antennas is the same except for the measured gain. The measured gain of the frusta matching layer is in very good agreement with simulations and is ∼1.6 dB higher than for the parylene-C matching layer, which is explained by the dielectric loss in the parylene-C. Although different types of parylene with lower dieletric loss than the parylene-C are available [27] (measured at low RF frequencies), the frusta matching layer has significant advantages as it operates over more than an octave bandwidth and it is fabricated using the same process as the lens array itself.

References

[1] D. F. Filipovic, S. S. Gearhart, and G. M. Rebeiz, "Double-slot antennas on extended hemispherical and elliptical silicon dielectric lenses," *IEEE Trans. Microw. Theory Techn.*, vol. 41, no. 10, pp. 1738–1749, Oct. 1993, doi: 10.1109/22.247919.

[2] N. Llombart, G. Chattopadhyay, A. Skalare, and I. Mehdi, "Novel terahertz antenna based on a silicon lens fed by a leaky wave enhanced waveguide," *IEEE Trans. Antennas Propag.*, vol. 59, no. 6, pp. 2160–2168, Jun. 2011, doi: 10.1109/TAP.2011.2143663.

[3] M. Alonso-delPino, C. Jung-Kubiak, T. Reck, N. Llombart, and G. Chattopadhyay, "Beam scanning of silicon lens antennas using integrated piezomotors at submillimeter wavelengths," *IEEE Trans. Terahertz Sci. Technol.*, vol. 9, no. 1, pp. 47–54, Jan. 2019, doi: 10.1109/TTHZ.2018.2881930.

[4] N. T. Nguyen, R. Sauleau, and C. J. Martinez Perez, "Very broadband extended hemispherical lenses: Role of matching layers for bandwidth enlargement," *IEEE Trans. Antennas Propag.*, vol. 57, no. 7, pp. 1907–1913, Jul. 2009, doi: 10.1109/TAP.2009.2021884.

[5] A. Neto, L. Borselli, S. Maci, and P. J. I. D. Maagt, "Input impedance of integrated elliptical lens antennas," *IEE Proc.- Microw., Antennas Propag.*, vol. 146, no. 3, pp. 181–186, Jun. 1999, doi: 10.1049/ip-map:19990336.

[6] A. J. Gatesman, J. Waldman, M. Ji, C. Musante, and S. Yagvesson, "An anti-reflection coating for silicon optics at terahertz frequencies," *IEEE Microw. Guided Wave Lett.*, vol. 10, no. 7, pp. 264–266, Jul. 2000, doi: 10.1109/75.856983.

[7] S. Sahin, N. K. Nahar, and K. Sertel, "Thin-film SUEX as an antireflection coating for mmW and THz applications," *IEEE Trans. Terahertz Sci. Technol.*, vol. 9, no. 4, pp. 417–421, Jul. 2019, doi: 10.1109/TTHZ.2019.2915672.

[8] J. Lau et al., "Millimeter-wave antireflection coating for cryogenic silicon lenses," *Appl. Opt.*, vol. 45, no. 16, pp. 3746–3751, Jun. 2006.

[9] T. Nitta et al., "Anti-reflection coating for cryogenic silicon and alumina lenses in millimeter-wave bands," *J. Low Temp. Phys.*, vol. 176, no. 5/6, pp. 677–683, 2014.

[10] A. Neto, S. Monni, and F. Nennie, "UWB, non dispersive radiation from the planarly fed leaky lens antenna—Part II: Demonstrators and measurements," *IEEE Trans. Antennas Propag.*, vol. 58, no. 7, pp. 2248–2258, Jul. 2010, doi: 10.1109/TAP.2010.2048880.

[11] T. Hasebe et al., "Development of multi-layer anti-reflection structures for millimeter-wave silicon optics using deep reactive ion etching process," *J. Low Temp. Phys.*, vol. 199, no. 1, pp. 339–347, Apr. 2020, doi: 10.1007/s10909-019-02286-4.

[12] F. Defrance et al., "1.6:1 bandwidth two-layer antireflection structure for silicon matched to the 190–310 GHz atmospheric window," *Appl. Opt.*, vol. 57, no. 18, pp. 5196–5209, 2018, doi: 10.1364/AO.57.005196.

[13] J. D. Wheeler et al., "Anti-reflection coatings for submillimeter silicon lenses," *Proc. SPIE*, vol. 9153, pp. 944–954, 2014.

[14] R. Datta et al., "Large-aperture wide-bandwidth antireflection-coated silicon lenses for millimeter wavelengths," *Appl. Opt.*, vol. 52, no. 36, pp. 8747–8758, Dec. 2013.

[15] P. Yagoubov et al., "Wideband 67–116 GHz receiver development for ALMA band 2," *Astron. Astrophys.*, vol. 634, no. A46, Feb. 2020, doi: 10.1051/0004-6361/201936777.

[16] J. E. Golec et al., "Design and fabrication of metamaterial anti-reflection 369 coatings for the simons observatory," in *Proc. Adv. Optical. Mech. Technol. Telescopes Instrum. IV*, 2020, vol. 114515T. [Online]. Available: https://doi.org/10.1117/12.2561720

[17] T. Nitta et al., "Design, fabrication and measurement of pyramid-type antireflective structures on columnar crystal silicon lens for millimeter-wave astronomy," *J. Low Temp. Phys.*, vol. 193, no. 5, pp. 976–983, Dec. 2018.

[18] K. Young et al., "Broadband millimeter-wave anti-reflection coatings on silicon using pyramidal sub-wavelength structures," *J. Appl. Phys.*, vol. 121, no. 21, Jun. 2017, Art. no. 213103.

[19] R. Takaku et al., "Large diameter millimeter-wave low-pass filter made of alumina with laser ablated anti-reflection coating," *Opt. Exp.*, vol. 29, pp. 41745–41765, 2021.

[20] M. Alonso-delPino, S. Bosma, C. Jung-Kubiak, G. Chattopadhyay, and N. Llombart, "Wideband multimode leaky-wave feed for scanning lens-phased array at submillimeter wavelengths," *IEEE Trans. Terahertz Sci. Technol.*, vol. 11, no. 2, pp. 205–217, Mar. 2021, doi: 10.1109/TTHZ.2020.3038033.

[21] O. Yurduseven, "Wideband integrated lens antennas for terahertz deep space investigation," Ph.D. thesis, Delft Univ. Technol., Delft, The Netherlands, 2016.

[22] H. Zhang, S. O. Dabironezare, G. Carluccio, A. Neto, and N. Llombart, "A Fourier optics tool to derive the plane wave spectrum of quasi-optical systems," *IEEE Antennas Propag. Mag.*, vol. 63, no. 1, pp. 103–116, Feb. 2021, doi: 10.1109/MAP.2020.3027233.

[23] A. Gonzalez, "Probe characterization in terahertz near-field beam measurement systems," *IEEE Trans. Terahertz Sci. Technol.*, vol. 6, no. 6, pp. 824–831, Nov. 2016, doi: 10.1109/TTHZ.2016.2607522.

[24] H.-W. Hübers et al., "Parylene anti-reflection coating of a quasi-optical hot-electron-bolometric mixer at terahertz frequencies," *Infrared Phys. Technol.*, vol. 42, no. 1, pp. 41–47, 2001.

[25] P. G. J. Irwin et al., "Investigation of dielectric spaced resonant mesh filter designs for PMIRR," *Infrared Phys.*, vol. 34, no. 6, pp. 549–563, Dec. 1993.

[26] A. J. Gatesman, J. Waldman, M. Ji, C. F. Musante, and S. Yagvesson, "An anti-reflection coating for silicon optics at terahertz frequencies," *IEEE Microw. Guided Wave Lett.*, vol. 10, no. 7, pp. 264–266, Jul. 2000.

[27] Specialty Coating Systems, "Parylene properties," 2007. Accessed: Apr. 3, 2022. [Online]. Available: https://www.physics.rutgers.edu/∼podzorov/parylene%20properties.pdf

Juan Bueno received the Graduate degree in physics from the University of Cantabria, Santander, Spain, in 2003 and the Ph.D. degree in physics from the University of Leiden, Leiden, The Netherlands, in 2007.

During his Ph.D. degree studies, he studied quantum crystals at very low temperatures. From 2007 to 2008, he was a Postdoctoral Fellow with the University of California, San Diego, CA, USA, continuing his work on quantum crystals. In 2008, he made the decision to switch research topics and interests from fundamental physics to the study of superconducting devices. He was a NASA Postdoctoral position (NPP), becoming a Post Doc with the Jet Propulsion Laboratory (USA) until 2010. During this time, he pioneered a new type of pair-breaking radiation detector, the Quantum Capacitance Detector. After his time with JPL, he joined the Center for Astrobiology (Spain) in 2010 after receiving a JAE-doc grant, working mainly on kinetic inductance detectors (KIDs). In 2012, he was an Instrument Scientist with SRON—Netherlands Institute for Space Research (The Netherlands), working on the development of KIDs for sub-mm wave and far IR space-based observatories. He is a high frequency RF Engineer with the ELCA Group, Technical University of Delft in 2021, working on the XG sensing and communications laboratories. He has authored or coauthhored more than 40 peer-reviewed papers, almost a third of them as the first author. His research interest concentrates on the development of over the air technology at sub-millimeter wave frequencies for detection and communication applications.

Sjoerd Bosma (Student Member, IEEE) received the B.Sc. and M.Sc. degrees (cum laude) in electrical engineering in 2015 and 2017, respectively, from the Delft University of Technology (TU Delft), Delft, The Netherlands, where he is currently working toward the Ph.D. degree with Terahertz Sensing Group.

From September 2018 to February 2019, he was a JPL Visiting Student Researcher Program with Jet Propulsion Laboratory, Pasadena, CA, USA. He is working on leaky-wave lens antenna arrays at (sub)millimeter-waves.

Tobias Bußkamp-Alda received the Graduate degree in electronics technician from SIEMENS, Bocholt, Germany, certified by the Chamber of Industry and Commerce (Germany) in 2004. After two years collecting practical experience, he studied Laser & Optical Technologies in Remagen (Germany).

For his Bachelor thesis, he was with the Fraunhofer Institute for Laser Technology ILT, Aachen Germany, working on the correction of the thermal focus shift at high power CO^2-TRUMPF-Lasers.

Since 2010, he chose the way of working in practical use of special laser systems at Veldlaser Innovations B.V., Heerenberg, The Netherlands. He got experience in laser drilling, welding and cutting, and specialised in the use of ultrashort pulsed laser systems. After two years of experience, he started to build his own laser systems to meet the high demands of Veldlaser's customers, such as NASA/JPL, SRON, COHERENT, SIEMENS, ASML.

One of his particular skills is the most advanced laser ablation setup to create different types of silicon lens arrays for IR-space based observatories. For this application aerospace customers from all over the world (USA, China, France, The Netherlands, Germany, and Finland) are in direct contact with Tobias to realize their developments.

Maria Alonso-delPino (Senior Member, IEEE) received the degree in telecommunications engineering and the Ph.D. degree in signal theory and communications/electrical engineering from the Technical University of Catalonia, Barcelona, Spain, in 2008 and 2013, respectively; and the M.S. degree in electrical engineering from the Illinois Institute of Technology, Chicago, IL, USA, in 2008.

From 2014 to 2015, she was as a Postdoctoral Researcher with the Technical University of Delft (TUDelft), Delft, Netherlands. From 2015 to 2016, she was a NASA postdoctoral fellow at the Jet Propulsion Laboratory, Pasadena, CA, USA. From 2016 to 2020, she was a Member of the technical staff with the Sub-millimeter Wave Advanced Technology group of JPL/NASA. Since 2020, she is currently an Assistant Professor with TUDelft. Her interests include millimeter and submillimeter-wave heterodyne and direct detection receiver technologies, antennas, quasi-optical systems.

Dr. Alonso-delPino was a co-recipient of the 2014 IEEE Terahertz Science and Technology Best Paper Award and the recipient of the Outstanding Reviewer Award of the IEEE TRANSACTIONS ON TERAHERTZ SCIENCE AND TECHNOLOGY in 2013, and the Best Theory and Design Antenna Paper award in the 16th European Conference on Antennas and Propagation in 2022.

Nuria Llombart (Fellow, IEEE) received the Master's degree in electrical engineering and the Ph.D. degree in electrical engineering from the Polytechnic University of Valencia, Valencia, Spain, in 2002 and 2006, respectively.

During her Master's degree studies, she spent one year at the Friedrich Alexander University of Erlangen Nuremberg, Erlangen, Germany, and with the Fraunhofer Institute for Integrated Circuits, Erlangen, Germany. From 2002 to 2007, she was with the Antenna Group, TNO Defense, Security and Safety Institute, The Hague, The Netherlands, working as a Ph.D. student and afterward as a Researcher. From 2007 to 2010, she was a Postdoctoral Fellow with the California Institute of Technology, working with the Submillimeter Wave Advance Technology Group, Jet Propulsion Laboratory, Pasadena, CA, USA. She was a "Ramón y Cajal" fellow in the Optics Department, Complutense University of Madrid, Madrid, Spain, from 2010 to 2012. In September 2012, she was with the THz Sensing Group, Technical University of Delft, Delft, The Netherlands, where as of February 2018 she is a Full Professor. She has coauthored more than 200 journal and international conference contributions in the areas of antennas and THz systems. Dr. Llombart was the co-recipient H. A. Wheeler Award for the Best Applications Paper of 2008 in the IEEE TRANSACTIONS ON ANTENNAS AND PROPAGATION, the 2014 THz Science and Technology Best Paper Award of the IEEE Microwave Theory and Techniques Society, and several NASA awards. She was also the recipient of the 2014 IEEE Antenna and Propagation Society Lot Shafai Mid-Career Distinguished Achievement Award. She was a Board Member of the IRMMW-THz International Society and an Associate Editor for the IEEE TRANSACTION ON ANTENNAS AND PROPAGATION. In 2015, she was the recipient of European Research Council Starting Grant. In 2019, she became an IEEE fellow for contributions to millimeter and submillimeter wave quasi-optical antennas.